RSC Advances

PAPER

View Article Online
View Journal | View Issue

Cite this: *RSC Adv.*, 2026, **16**, 9371

Microwave-assisted N,S doped carbon quantum dots as fluorescent nanoprobes for vibegron determination: face-centered design optimization, validation, and green chemistry assessment

Humood Al Shmrany,[a] Ali Alqahtani,[b] Taha Alqahtani,[b] Adil Alshehri[c] and Ahmed A. Almrasy *[d]

A novel, sensitive, and environmentally sustainable spectrofluorimetric method was developed for vibegron quantification in pharmaceutical formulations and biological matrices using nitrogen and sulfur co-doped carbon quantum dots (N,S CQDs) as fluorescent nanoprobes. The N,S-CQDs were synthesized *via* rapid microwave-assisted green chemistry and comprehensively characterized through transmission electron microscopy, dynamic light scattering, Fourier-transform infrared spectroscopy, ultraviolet-visible absorption spectroscopy, and fluorescence spectroscopy, revealing optimal excitation and emission wavelengths at 344 nm and 418 nm, respectively. Mechanistic investigation demonstrated that vibegron induced concentration-dependent fluorescence quenching through static complex formation, as evidenced by decreasing Stern–Volmer constants with increasing temperature (9.68×10^5 to 6.86×10^5 M^{-1}). Thermodynamic analysis revealed spontaneous binding ($\Delta G° = -34.70$ kJ mol^{-1}) driven by electrostatic interactions and hydrogen bonding, with negative enthalpy and positive entropy. Critical experimental parameters were systematically optimized using face-centered central composite design, revealing a significant reduced quadratic model ($R^2 = 0.9866$) with optimal values identified and further employed for method validation. The method was rigorously validated according to ICH Q2 (R2) guidelines, demonstrating excellent linearity (30–1500 ng mL^{-1}, $r^2 = 0.9998$), high sensitivity (LOD 9.85 ng mL^{-1}, LOQ 29.54 ng mL^{-1}), superior accuracy (100.88 ± 1.34%) and precision (repeatability 1.33%, intermediate precision 1.74%). Successful application to commercial tablets yielded 100.07 ± 0.81% content with statistical equivalence to established HPLC methods confirmed through *t*-test, *F*-test, and interval hypothesis testing. Furthermore, spiked human plasma analysis demonstrated recoveries ranging from 96.44% to 104.28% with RSD values below 4%, confirming applicability to biological matrices for therapeutic drug monitoring. Comprehensive green chemistry assessment using AGREE (0.65), CaFRI (80/100), and BAGI (70.0/100) metrics demonstrated favorable environmental sustainability characterized by minimal hazardous reagent consumption, low carbon footprint, reduced waste generation, and excellent practical applicability, providing an environmentally benign analytical tool for routine pharmaceutical quality control and therapeutic drug monitoring applications.

Received 19th November 2025
Accepted 6th February 2026

DOI: 10.1039/d5ra08942e

rsc.li/rsc-advances

1. Introduction

Overactive bladder (OAB) represents a multifaceted symptom syndrome characterized by urinary urgency, frequently accompanied by increased urinary frequency, nocturia, and urgency urinary incontinence, in the absence of underlying pathological conditions.[1] The prevalence of OAB is substantial, affecting approximately 546 million individuals globally, with prevalence rates reaching 17.4% in men and 16.0% in women.[2,3] This chronic condition imposes considerable burdens on patients' health-related quality of life and healthcare systems, with annual management costs estimated at 7 billion euros in Europe and 66 billion USD in the United States.[4] Vibegron, a second-generation β3-adrenergic receptor agonist approved by the United States Food and Drug Administration in 2020, has emerged as a therapeutic alternative to traditional anti-muscarinic agents for OAB management.[3] Structurally, vibegron exhibits a lower molecular weight (445 Da), higher lipophilicity,

[a]*Department of Medical Laboratory, College of Applied Medical Sciences, Prince Sattam bin Abdulaziz University, Alkharj, 11942, Saudi Arabia*
[b]*Department of Pharmacology, College of Pharmacy, King Khalid University, Abha, 62529, Saudi Arabia*
[c]*Department of Medicine, College of Medicine, King Khalid University, Abha, 62529, Saudi Arabia*
[d]*Pharmaceutical Analytical Chemistry Department, Faculty of Pharmacy, Al-Azhar University, Cairo 11751, Egypt. E-mail: ahmedalialmrasy8@gmail.com*

and superior β3-adrenoceptor selectivity (>7937-fold over β1 and >9000-fold over β2 adrenoceptors) compared to first-generation β3-agonists.[5,6] The compound exerts its therapeutic effects through selective activation of β3-adrenoceptors localized in the detrusor smooth muscle and urothelium, thereby facilitating bladder relaxation during the storage phase of the micturition cycle without compromising voiding function.[7,8] Following oral administration of the standard 75 mg dose, vibegron demonstrates favorable pharmacokinetic properties, including rapid absorption with peak plasma concentrations achieved within 1–3 hours, a prolonged terminal elimination half-life of 60–70 hours supporting once-daily dosing, and minimal cytochrome P450-mediated metabolism, thereby reducing the potential for clinically significant drug-drug interactions.[9,10] Furthermore, preclinical investigations have confirmed that vibegron does not penetrate the central nervous system, substantially mitigating the risk of cognitive adverse effects commonly associated with anticholinergic therapies.[11] Despite the growing clinical utilization of vibegron and the critical importance of therapeutic drug monitoring for optimizing treatment outcomes, bioanalytical methods for its quantification in pharmaceutical formulations and biological matrices remain limited.[5] Consequently, the development of sensitive, selective, and validated analytical methodologies is essential to support pharmacokinetic studies, bioequivalence trials, quality control assessments, and routine therapeutic monitoring of vibegron.

To date, analytical methodologies for vibegron quantification remain limited, with only a few validated approaches reported in the literature.[12] High-performance liquid chromatography coupled with photodiode array detection (HPLC-PDA) has been developed for vibegron quantification in pharmaceutical formulations using C18 stationary phases with acetonitrile-based mobile phases at 248 nm detection, achieving linearity ranges of 2.5–200 μg mL^{-1} and limits of quantification between 1.2 and 1.9 μg mL^{-1}.[12,13] However, these methods exhibit limited sensitivity, require toxic organic solvents in substantial volumes, necessitate extended analysis times, and impose high operational costs due to expensive instrumentation and maintenance requirements.[12,13] Liquid chromatography-tandem mass spectrometry (LC-MS/MS) methods have been reported for vibegron quantification in human plasma, utilizing gradient elution with formic acid-modified mobile phases and positive electrospray ionization, achieving superior sensitivity with limits of quantification as low as 0.5 ng mL^{-1}.[5] Despite enhanced sensitivity, LC-MS/MS methods demand highly sophisticated and costly instrumentation, require specialized technical expertise, involve complex sample preparation procedures including protein precipitation, and are not readily accessible in routine quality control laboratories.[5] Additionally, a spectrofluorimetric method based on derivatization with dansyl chloride has been developed, demonstrating detection limits of 3.6 ng mL^{-1}.[14] Nevertheless, this approach involves multi-step derivatization procedures with prolonged reaction times (12 minutes), utilizes hazardous reagents including methylene chloride for extraction, and introduces additional sources of analytical variability.[14] These limitations collectively underscore the critical need for developing alternative analytical platforms that combine high sensitivity, operational simplicity, rapid analysis, cost-effectiveness, minimal environmental impact, and suitability for routine quality control and therapeutic monitoring applications.

To overcome these limitations of conventional chromatographic techniques—particularly the dependence on toxic solvents, complex instrumentation, extended analysis times, high costs, and substantial environmental impact—alternative detection strategies based on fluorescence sensing have emerged as promising solutions. This technique has gained considerable attention in pharmaceutical analysis due to its inherent advantages of high sensitivity, operational simplicity, cost-effectiveness, minimal sample consumption, and rapid analysis capabilities.[15,16] Among different fluorescent fluorophores, carbon quantum dots (CQDs) specifically address the identified chromatographic limitations by enabling aqueous-based detection without organic solvents, utilizing simple and affordable instrumentation, providing rapid analysis within minutes, and achieving sensitivity comparable to LC-MS/MS while maintaining excellent environmental sustainability. These nanomaterials have emerged as promising alternatives to traditional semiconductor quantum dots, offering distinct advantages including low toxicity, excellent biocompatibility, high chemical stability, superior photostability, tunable photoluminescence, and environmentally benign composition.[17–19] The optical properties and analytical performance of CQDs can be significantly enhanced through heteroatom doping strategies, wherein the introduction of foreign atoms into the carbon framework modulates the electronic structure, creates additional surface defects, and introduces abundant functional groups.[20,21] Nitrogen and sulfur co-doping (N,S CQDs) has demonstrated particular efficacy in improving photoluminescence quantum yields, with reported values reaching up to 73%, substantially higher than undoped CQDs.[22,23] The synergistic effect of nitrogen and sulfur doping arises from their comparable atomic sizes and electronegativity values relative to carbon, facilitating uniform incorporation while generating additional coordination sites and electron-donating capabilities that promote radiative recombination processes.[24,25] Microwave-assisted synthesis has emerged as a preferred green chemistry approach for N,S CQD fabrication, offering advantages of rapid reaction times, energy efficiency, uniform heating, high product yields, and minimal use of hazardous solvents compared to conventional hydrothermal methods.[26] Recent advances in microwave-assisted N,S CQD synthesis have demonstrated ultrafast synthesis protocols achieving high quantum yields within 1.5–5 minutes using diverse precursor combinations.[27,28] These combinations include citric acid-based systems with sulfur and nitrogen co-dopants achieving quantum yields up to 24% in 4 minutes at 800 W,[27] β-cyclodextrin-melamine-thiourea systems producing 24% quantum yield particles,[29] biomass-derived approaches using natural sulfur and nitrogen sources from plant materials,[28] and optimized sucrose-urea-thiourea systems producing N,S-CDs in approximately 4 minutes.[30] These recent methodological

advances confirm that microwave-assisted synthesis represents the most efficient green chemistry route for producing highly fluorescent N,S CQDs suitable for pharmaceutical analytical applications.[31] Hence, N,S CQDs-based fluorescent sensing platforms have been successfully applied to pharmaceutical analysis, demonstrating sensitive and selective detection of various analytes including antibiotics, vitamins, and therapeutic agents in complex matrices.[32,33]

To date, no analytical methods have been reported for vibegron determination using N,S CQDs as fluorescent nanoprobes. Therefore, this work represents the first application of microwave-assisted N,S CQDs as fluorescent nanoprobes for vibegron analysis, offering a novel, sensitive, and environmentally sustainable alternative to the limited conventional chromatographic methods. The specific objectives of this study include: (1) synthesis of N,S CQDs using a rapid microwave-assisted green chemistry approach and comprehensive characterization of their morphological, chemical, and optical properties; (2) investigation of the fluorescence quenching mechanism between N,S CQDs and vibegron through Stern–Volmer kinetic analysis and thermodynamic parameter evaluation; (3) systematic optimization of critical experimental parameters including pH, buffer volume, N,S CQDS concentration, and incubation time using face-centered central composite design; (4) validation of the developed spectrofluorimetric method according to ICH Q2 (R2) guidelines; (5) application of the validated method to vibegron quantification in commercial pharmaceutical formulations and biological matrices with statistical comparison to established chromatographic techniques; and (6) evaluation of the environmental sustainability and greenness profile of the developed methodology using recent assessment tools. This work provides a practical, cost-effective, and environmentally benign analytical tool for vibegron quantification that can be adopted for its routine quality control laboratories and extended to its therapeutic drug monitoring programs, thereby contributing to the advancement of green analytical methodologies in pharmaceutical analysis.

2. Experimental

2.1. Chemicals and reagents

Vibegron reference standard (99.12% purity) was obtained from Sigma-Aldrich (St. Louis, MO, USA). High-purity reagents for N,S CQDS synthesis including citric acid monohydrate and *N*-acetyl-L-cysteine were procured from Piochem (Cairo, Egypt). HPLC-grade ethanol and acetonitrile were sourced from Merck (Darmstadt, Germany). Quinine sulfate dihydrate for quantum yield determination was purchased from Sigma-Aldrich (St. Louis, MO, USA). Analytical-grade chemicals including orthophosphoric acid, boric acid, glacial acetic acid, sodium hydroxide, and sulfuric acid were obtained from El-Nasr Pharmaceutical Chemicals Co. (Cairo, Egypt). Potassium bromide for FTIR analysis was purchased from Merck (Darmstadt, Germany). Commercial vibegron tablets (Gemtesa®, 75 mg per tablet, Urovant Sciences, Irvine, CA, USA) were procured from the United States pharmaceutical market. Distilled water was utilized throughout all experimental procedures. Human plasma samples were procured from VACSERA CO. (Giza, Egypt), stored at −20 °C, and thawed at room temperature prior to analysis.

Britton–Robinson universal buffer systems were freshly prepared for each analytical session by combining equimolar amounts (0.04 M each) of orthophosphoric acid, boric acid, and glacial acetic acid in ultrapure water. pH adjustment across the range of 3.0–8.0 was achieved using standardized 0.2 M sodium hydroxide solution. All buffer pH values were verified using a calibrated pH meter to maintain accuracy within ±0.05 pH units.

2.2. Instrumentation

A Shimadzu UV-1800 double-beam spectrophotometer was utilized for recording ultraviolet-visible absorption spectra in the wavelength range of 200–800 nm using 1 cm path length quartz cuvettes. Fluorescence emission and excitation spectra were acquired using a Jasco FP-6200 spectrofluorometer fitted with a 150 W xenon lamp. The instrument operated with both excitation and emission bandpass filters set to 10 nm, a scanning rate of 4000 nm min^{-1}, and fluorescence emission monitored between 365 and 600 nm. Quartz cells with 1 cm optical path length and four polished faces were employed for all fluorometric determinations. A Jenway 3505 pH meter with a glass combination electrode was used for pH measurements. Daily calibration of the pH electrode was performed using certified reference buffers.

Microwave-assisted synthesis of the N,S CQDs was conducted using a Tornado domestic microwave oven (1000 W, Egypt). Centrifugation procedures were performed on a Hettich benchtop centrifuge (Tuttlingen, Germany). N,S CQDs particles morphology and size were examined by transmission electron microscopy using a JEOL JEM-2100 instrument at 200 kV accelerating voltage. A Malvern Zetasizer Nano ZS system was employed for hydrodynamic diameter determination and size distribution analysis through dynamic light scattering measurements. Chemical structure elucidation was performed by Fourier-transform infrared spectroscopy using a Nicolet iS5 spectrometer. Spectra were collected from 4000 to 400 cm^{-1} using samples prepared as compressed potassium bromide discs.

2.3. Synthesis and characterization of N,S CQDs

N,S CQDs were synthesized using a rapid microwave-assisted green chemistry approach based on reported literature with modifications.[34–38] Briefly, 0.38 g (2 mmol) of citric acid monohydrate and 0.32 g (2 mmol) of *N*-acetyl-L-cysteine were dissolved in 20 mL of ultrapure water in a 50 mL Pyrex glass beaker under magnetic stirring for 5 minutes until complete dissolution was achieved. The clear solution in the uncovered beaker was placed at the center of the turntable in a domestic microwave oven (700 W) for 5 minutes. The beaker was positioned at the center of the rotating turntable to ensure uniform microwave field exposure throughout the reaction. During the reaction, the initially colorless solution gradually turned yellow and subsequently brown, indicating the formation of carbon

quantum dots. After cooling to room temperature, the crude product was centrifuged at 10 000 rpm for 15 minutes to remove large particulate aggregates. The supernatant was collected and purified by dialysis using a cellulose membrane with a molecular weight cutoff of 1000 Da against ultrapure water for 24 hours, with water being replaced every 6 hours. The purified N,S CQD solution was precipitated by adding excess cold ethanol (1 : 3 v/v ratio)[39] followed by centrifugation at 10 000 rpm for 20 minutes. The resulting precipitate was washed twice with ethanol to remove residual impurities and dried under vacuum at 40 °C to obtain N,S CQDs as a brown powder. A stock solution of N,S CQDs was prepared by accurately weighing the dried powder and dissolving it in ultrapure water to achieve a concentration of 1.0 mg mL^{-1}. The stock solution was stored in amber glass vials at 4 °C in the dark, maintaining fluorescence stability for at least three months.

The morphological, chemical, and optical properties of the synthesized N,S CQDs were comprehensively characterized using multiple analytical techniques. Transmission electron microscopy (TEM) analysis was performed to determine the particle size and morphology of N,S CQDs. Samples for TEM analysis were prepared by placing a drop of diluted N,S CQD ethanolic solution onto carbon-coated copper grids and allowing them to air-dry at room temperature. The hydrodynamic diameter and size distribution of N,S CQDs in aqueous solution were evaluated by dynamic light scattering (DLS) measurements at 25 °C. Chemical characterization was conducted using Fourier-transform infrared (FTIR) spectroscopy in the wavenumber range of 4000–400 cm^{-1} to identify surface functional groups. N,S CQD powder was mixed with potassium bromide and pressed into pellets for FTIR measurements. Optical characterization included ultraviolet-visible (UV-vis) absorption spectroscopy performed in the wavelength range of 200–500 nm using quartz cuvettes with 1 cm path length. Fluorescence measurements were conducted with excitation and emission slit widths of 10 nm. The quantum yield of N,S CQDs was evaluated using the single-point comparative method with quinine sulfate in 0.1 M H_2SO_4 (quantum yield = 0.54) as the reference standard. Both samples were excited at 344 nm with absorbance maintained below 0.1 to avoid inner filter effects. The quantum yield was calculated according to the equation: $QY_{sample} = QY_{ref} \times (I_{sample}/I_{ref}) \times (A_{ref}/A_{sample}) \times (\eta_{sample}/\eta_{ref})$,[2] where I is the integrated fluorescence intensity, A is the absorbance at excitation wavelength, and η is the refractive index of the solvent.

2.4. Experimental design and optimization

A face-centered central composite design was employed to systematically optimize critical experimental parameters affecting the analytical performance of the N,S CQD-based fluorescence quenching method. Based on preliminary experiments, four independent variables were identified as significant factors: pH (Factor *A*), buffer volume in mL (Factor *B*), N,S CQDS concentration in μg mL^{-1} (Factor *C*), and incubation time in minutes (Factor *D*). Each factor was investigated at three levels: low (−1), center (0), and high (+1). The experimental design comprised 27 runs including factorial points, axial points, and center point replicates to evaluate main effects, interactions, and quadratic terms (Table S1).

For each experimental run, the general analytical procedure was followed. Briefly, appropriate volumes of Britton–Robinson buffer at the designated pH, N,S CQD stock solution at the specified concentration, and vibegron standard solution were mixed in a 10 mL volumetric flask and diluted to volume with distilled water. The mixture was incubated for the predetermined time at room temperature (25 ± 2 °C) in the dark, then transferred to a quartz cuvette for fluorescence measurement. The fluorescence quenching factor (F_0/F), where F_0 represents the fluorescence intensity of N,S CQDs alone and F represents the fluorescence intensity of N,S CQDs in the presence of vibegron, was selected as the response variable.

Design Expert® software (version 11, Stat-Ease Inc., Minneapolis, MN, USA) was utilized for experimental design generation, statistical analysis, and response surface modeling. Analysis of variance (ANOVA) was performed to evaluate the statistical significance of model terms, with p-values < 0.05 considered statistically significant. The adequacy of the developed model was assessed through coefficient of determination (R^2), adjusted R^2, predicted R^2, and adequate precision values. Response surface plots were constructed to visualize the relationship between factors and response, facilitating identification of optimal experimental conditions.

2.5. General analytical procedure and construction of calibration curve

Based on the optimized experimental conditions obtained from the face-centered central composite design, the following analytical procedure was established for vibegron determination. Into a series of 10 mL volumetric flasks, aliquots of vibegron working standard solutions were transferred to achieve final concentrations ranging from 30 to 2000 ng mL^{-1}. To each flask, 1.0 mL of Britton–Robinson buffer (pH 5.6) and 1.35 mL of N,S CQD stock solution (final concentration 135 μg mL^{-1}) were added. The solutions were diluted to volume with distilled water and mixed thoroughly. The mixtures were incubated at room temperature (25 ± 2 °C) in the dark for 3.0 min to allow complete interaction between N,S CQDs and vibegron. Following incubation, the solutions were transferred to 1 cm quartz cuvettes for fluorescence measurements. Fluorescence intensity was recorded at 344/418 nm (excitation/emission wavelengths).

A blank solution containing only N,S CQDs without vibegron was prepared following the same procedure to obtain the initial fluorescence intensity (F_0). The fluorescence quenching factor (F_0/F) was calculated for each vibegron concentration, where F represents the fluorescence intensity in the presence of vibegron. The calibration curve was constructed by plotting the fluorescence quenching factor (F_0/F) against the corresponding vibegron concentration (ng mL^{-1}). Linear regression analysis was performed to establish the relationship between F_0/F and vibegron concentration within the working range of 30–2000 ng mL^{-1}.

2.6. Application to pharmaceutical formulations and biological samples

2.6.1 Analysis of pharmaceutical formulations. Ten commercial Gemtesa® tablets were accurately weighed and

grounded to a fine homogeneous powder. An accurately weighed quantity of the powder equivalent to 10 mg of vibegron was transferred into a 100 mL volumetric flask containing approximately 60 mL of ethanol. The flask was subjected to ultrasonication for 20 minutes to achieve quantitative extraction of vibegron. After cooling to ambient temperature, the volume was completed with ethanol and the solution was filtered through Whatman no. 42 filter paper, discarding the initial filtrate portion. The resulting ethanolic stock solution (100 μg mL^{-1}) was appropriately diluted with distilled water to prepare working solutions. Quantification was performed following the optimized analytical procedure outlined in Section 2.5, with vibegron concentration determined *via* the calibration curve regression equation.

2.6.2 Analysis of spiked human plasma samples. Plasma samples were thawed at ambient temperature and vortexed for 30 seconds to ensure homogeneity. Aliquots of drug-free plasma were fortified with vibegron standard solution to yield final concentrations of 50, 100, 300, and 600 ng mL^{-1}. Deproteinization was accomplished by introducing 2 mL of chilled acetonitrile to each aliquot, followed by vigorous vortex agitation for 2 minutes. The mixtures were centrifuged at 10 000 rpm for 10 minutes at 4 °C. The clear supernatants were carefully separated and concentrated to dryness using a nitrogen stream at 40 °C. Each residue was redissolved in 500 μL of distilled water with thorough vortex mixing for 1 minute, then filtered through 0.22 μm syringe filters. The filtered samples were subsequently analyzed following the general analytical procedure with appropriate matrix-matched calibration standards. Percent recovery values were determined by correlating measured concentrations against theoretical spiked levels.

2.7 Green chemistry assessment

The environmental sustainability profile of the developed spectrofluorimetric method was systematically evaluated through three distinct assessment frameworks that collectively address environmental impact, carbon emissions, and practical feasibility.

AGREE assessment[40] provides a comprehensive evaluation framework based on twelve fundamental principles of sustainable analytical chemistry. The tool converts diverse experimental parameters into normalized scores ranging from 0 (non-compliant) to 1 (fully compliant) for each principle, covering aspects such as sample handling requirements, measurement location, procedural complexity, degree of automation, chemical derivatization needs, waste production, analytical throughput, energy requirements, reagent origins, chemical hazards, and analyst safety considerations. Final scores are mathematically derived from individual principle evaluations and displayed *via* a circular pictogram employing traffic-light coloring to indicate performance levels. Assessment was conducted using the desktop application available at mostwiedzy.pl/AGREE.

CaFRI assessment[41] quantifies the carbon footprint associated with analytical workflows through systematic evaluation of greenhouse gas emission contributors. The framework examines both direct emission sources (instrumental energy consumption, carbon dioxide generation factors) and indirect emission pathways (specimen storage conditions, transport logistics, staffing requirements, waste handling practices, material recycling implementation, and consumable usage patterns). Individual criterion performance is converted to numerical values that aggregate into a composite index spanning 0–100, with elevated scores reflecting reduced environmental impact. Visual representation employs a foot-shaped diagram with chromatic zones indicating performance categories. Web-based evaluation was performed *via* bit.ly/CaFRI.

BAGI assessment[42] evaluates the practical applicability of analytical procedures through ten operational characteristics encompassing measurement objectives, instrumental sophistication, processing capacity, workflow automation, parallel sample handling capability, preparatory procedure complexity, specimen quantity demands, concentration enhancement requirements, per-sample economics, and consumable accessibility. Each characteristic receives a numerical rating from 0–10 based on defined performance criteria, yielding cumulative scores between 0–100. Results visualization utilizes a star-shaped graphic with radial segments corresponding to individual evaluated parameters. Assessment employed software accessible at https://mostwiedzy.pl/en/justyna-plotka-wasylka,647762-1/BAGI and the web interface at https://bagi-index.anvil.app/.

3. Results and discussion

3.1 Characterization of N,S CQDs

The synthesis conditions for N,S CQDs were initially optimized to achieve maximum fluorescence quantum yield, which serves as a critical indicator of nanoprobe performance in analytical applications. N,S co-doping was specifically selected over single heteroatom doping based on its superior photoluminescence performance demonstrated in comparative literature studies.[31,43,44] While single nitrogen-doped CQDs typically achieve quantum yields of 5.2–9.6% and single sulfur-doped CQDs exhibit even lower values of 0.33–3.09%, N,S co-doped systems demonstrate remarkable quantum yields reaching 51–73%. This substantial enhancement arises from synergistic mechanisms wherein sulfur incorporation facilitates increased nitrogen doping concentration while both heteroatoms collectively create electron-donating surface states that enhance radiative recombination processes. Based on this rationale, the synthesis parameters including microwave power, irradiation time, and precursor molar ratio were systematically investigated to maximize quantum yield. Microwave power was systematically varied (500 W, 700 W, 900 W, and 1000 W) at a fixed irradiation time of 5 minutes to evaluate its effect on quantum yield. Powers below 700 W resulted in incomplete carbonization with lower quantum yields, while powers above 700 W caused excessive carbonization leading to aggregation and reduced fluorescence. At the optimal power of 700 W, irradiation time was then systematically investigated (3, 5, 7, and 10 minutes). Irradiation for 3 minutes yielded incomplete reaction with quantum yield of 38.2%, while extended times of 7 and 10

minutes resulted in over-carbonization with decreased quantum yields of 42.1% and 35.6%, respectively, accompanied by darker coloration indicating excessive graphitization. Additionally, the molar ratio of citric acid monohydrate to *N*-acetyl-L-cysteine was optimized by investigating ratios of 3 : 1, 2 : 1, 1 : 1, 1 : 2, and 1 : 3. The equimolar ratio (1 : 1, corresponding to 2 : 2 mmol in the synthesis) provided the highest quantum yield, as deviation from this ratio resulted in either insufficient nitrogen and sulfur doping (citric acid excess) or incomplete carbonization (*N*-acetyl-L-cysteine excess), both leading to reduced fluorescence quantum yields. The optimal synthesis conditions were established at 700 W microwave power for 5 minutes using equimolar amounts of citric acid monohydrate and *N*-acetyl-L-cysteine (2 : 2 mmol ratio). To ensure reproducibility despite using a domestic microwave oven, synthesis was performed in triplicate under the optimized standardized conditions (centered beaker placement, fixed 700 W power, controlled 5 minutes time). The quantum yields of three independent batches were 51.36%, 50.82%, and 51.91% (mean: 51.36 ± 0.55%, RSD = 1.06%), confirming excellent batch-to-batch reproducibility. These quantum yield values are comparable to previously reported N,S-doped CQDs synthesized through microwave-assisted approaches,[30] demonstrating the effectiveness of the rapid green chemistry synthesis protocol. The relatively high quantum yield can be attributed to the synergistic effect of nitrogen and sulfur co-doping, which introduces additional surface defects and electron-donating functional groups that enhance radiative recombination processes.[24,25]

Morphological characterization by transmission electron microscopy revealed that the synthesized N,S CQDs possessed quasi-spherical morphology with uniform size distribution (Fig. 1A). Statistical analysis of particle size measurements from TEM images indicated a mean particle diameter of 3.23 ± 1.41 nm, confirming the successful formation of quantum dots in the nanometer range. The narrow size distribution demonstrates the homogeneity of the synthesized nanomaterial, which is essential for reproducible analytical performance. Dynamic light scattering measurements yielded a mean hydrodynamic diameter of 3.76 ± 1.4 nm (Fig. 1B), which showed reasonable agreement with the TEM-derived particle size. The close correspondence between DLS and TEM measurements indicates minimal aggregation and excellent colloidal stability of the N,S CQDs in aqueous solution. The slight difference observed can be attributed to the hydration layer surrounding the nanoparticles in aqueous dispersion, as DLS measures the hydrodynamic radius including the solvation shell, whereas TEM provides the actual particle core diameter in the dried state. The small hydrodynamic diameter confirmed excellent aqueous dispersibility and colloidal stability of the N,S CQDs, which are crucial properties for fluorescence-based sensing applications.

Chemical characterization by Fourier-transform infrared spectroscopy provided comprehensive information regarding surface functional groups present on the N,S CQDs (Fig. 1C).

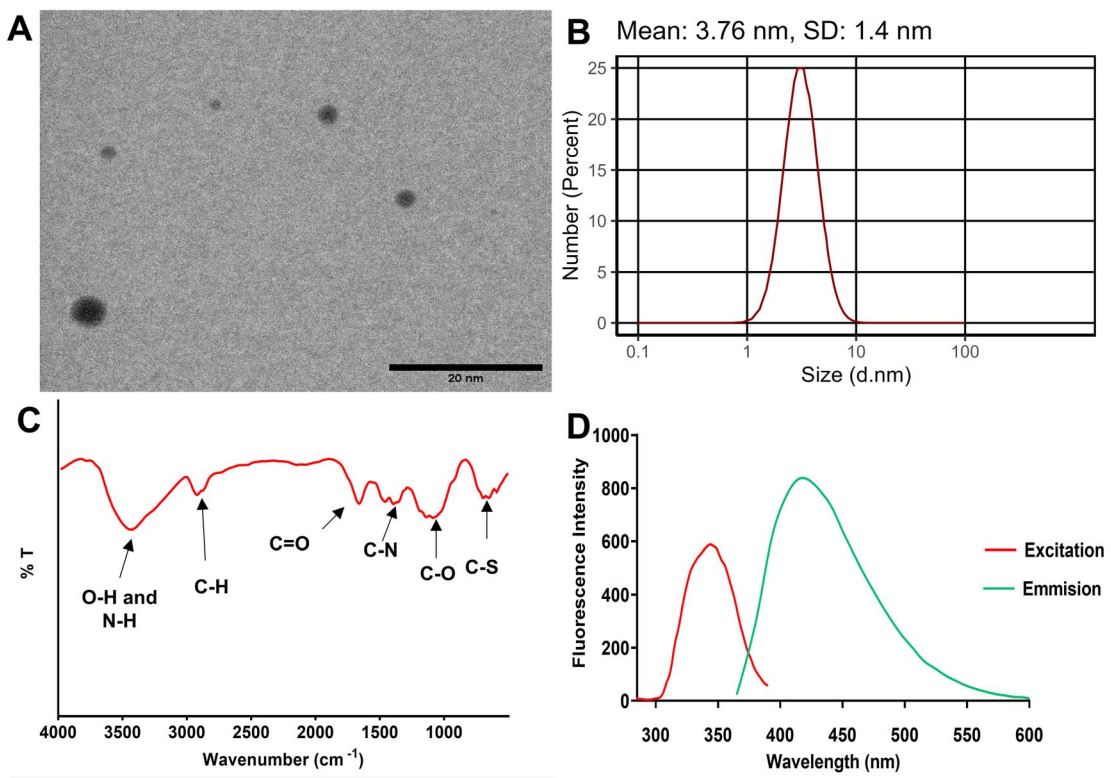

Fig. 1 (A) Transmission electron microscopy (TEM) image showing quasi-spherical morphology of N,S CQDs with scale bar of 20 nm; (B) Dynamic light scattering (DLS) size distribution histogram displaying mean hydrodynamic diameter of 3.76 ± 1.4 nm; (C) Fourier-transform infrared (FTIR) spectrum showing characteristic functional groups stretching vibrations; (D) Fluorescence excitation (red line) and emission (green line) spectra of N,S-CQDs in aqueous solution, showing excitation maximum at 344 nm and emission maximum at 418 nm.

The broad absorption band observed in the region of 3200–3600 cm^{-1} was assigned to overlapping O–H and N–H stretching vibrations, indicating the presence of hydroxyl and amino groups on the CQD surface. The peaks at approximately 2915 and 2860 cm^{-1} corresponded to aliphatic C–H stretching vibrations derived from the organic precursors. A prominent absorption band at 1652 cm^{-1} was attributed to C=O stretching vibrations, while the peak at 1380 cm^{-1} indicated C–N stretching vibrations, confirming successful nitrogen doping into the carbon framework. Additionally, the characteristic absorption band at 1067 cm^{-1} was assigned to C–O stretching vibrations, and the weak band at approximately 650 cm^{-1} corresponded to C–S stretching vibrations, providing evidence for sulfur incorporation. The presence of abundant oxygen-, nitrogen-, and sulfur-containing functional groups on the CQD surface contributes to excellent water solubility, enhanced fluorescence properties, and provides multiple interaction sites for analyte recognition.

Optical characterization commenced with ultraviolet-visible absorption spectroscopy (Fig. S1). The UV-vis absorption spectrum exhibited a characteristic absorption maximum at 338 nm, which can be attributed to n–π^* transitions of C=O and C=N bonds present in the aromatic domains of the carbon quantum dots. The absorption profile showed gradual decrease toward longer wavelengths with negligible absorption beyond 450 nm, which is typical for nitrogen- and sulfur-doped CQDs. Fluorescence spectroscopic investigation revealed optimal excitation and emission wavelengths at 344 nm and 418 nm, respectively (Fig. 1D), yielding a Stokes shift of 74 nm. This substantial Stokes shift minimizes self-absorption and inner filter effects, thereby enhancing the sensitivity and reliability of fluorescence measurements. The emission spectrum displayed a symmetric Gaussian-like profile with bright blue fluorescence under UV irradiation, consistent with quantum confinement effects and surface state emissions characteristic of carbon quantum dots. The photoluminescence properties exhibited excellent photostability under UV irradiation, demonstrating the suitability of these N,S CQDs as robust fluorescent nanoprobes for pharmaceutical analysis. Moreover, the stability of the synthesized N,S CQDs was evaluated to assess their suitability for routine analytical applications. Storage stability was investigated by monitoring the fluorescence intensity of N,S CQD stock solution (1.0 mg mL^{-1}) stored at 4 °C in amber glass vials over a period of 10 days. The fluorescence intensity remained stable with less than 4% variation, demonstrating adequate storage stability for routine analytical use during method validation and sample analysis.

3.2 Fluorescence quenching mechanism and thermodynamic studies

The interaction between N,S CQDs and vibegron was investigated through systematic fluorescence quenching studies. Fig. 2A illustrates the fluorescence emission spectra of N,S CQDs in the presence of increasing vibegron concentrations ranging from 0 to 2000 ng mL^{-1}. Upon incremental addition of vibegron, a progressive decrease in fluorescence intensity at 418 nm was observed without any significant shift in the emission maximum wavelength, indicating effective quenching of N,S CQDS fluorescence. This concentration-dependent quenching behavior formed the basis for the quantitative determination of vibegron. To elucidate the underlying quenching mechanism, various possible pathways were systematically evaluated. Inner filter effect (IFE) was first excluded as a potential mechanism by examining the UV-vis absorption spectrum of vibegron (Fig. S2). The absorption spectrum of vibegron exhibited absorption maxima at approximately 207 nm and 250 nm, with negligible absorption in the excitation (344 nm) and emission (418 nm) wavelength regions of the N,S CQDs. This absence of spectral overlap between the absorption spectrum of vibegron and the excitation/emission spectra of N,S CQDs effectively rules out IFE as the predominant quenching mechanism. Furthermore, Förster resonance energy transfer (FRET) was eliminated as a possible mechanism due to insufficient spectral overlap between the emission spectrum of N,S CQDs (donor) and the absorption spectrum of vibegron (acceptor), as the Förster distance requirement for efficient energy transfer was not satisfied. These findings collectively indicated that the fluorescence quenching arose from direct molecular interactions between vibegron and N,S CQDs rather than from optical interference or energy transfer processes.

To differentiate between static and dynamic quenching mechanisms, temperature-dependent fluorescence measurements were conducted at three different temperatures (298, 303, and 313 K). The Stern–Volmer equation ($F_0/F = 1 + K_{sv}[Q]$) was employed to analyze the quenching data, where F_0 and F represent the fluorescence intensities in the absence and presence of quencher, respectively, $[Q]$ denotes the quencher concentration, and K_{sv} is the Stern–Volmer quenching constant. Linear Stern–Volmer plots were obtained at all three temperatures (Fig. 2B), with correlation coefficients exceeding 0.99, indicating a single class of fluorophore binding sites. The calculated K_{sv} values decreased progressively with increasing temperature (9.68×10^5 M^{-1} at 298 K, 8.65×10^5 M^{-1} at 303 K, and 6.86×10^5 M^{-1} at 313 K), as summarized in Table 1. This inverse relationship between K_{sv} and temperature is characteristic of static quenching, wherein ground–state complex formation between the fluorophore and quencher predominates. In contrast, dynamic quenching typically exhibits increasing K_{sv} values with rising temperature due to enhanced molecular collision frequency. To further substantiate the static quenching mechanism, the bimolecular quenching rate constant (K_q) was calculated using the equation $K_q = K_{sv}/\tau_0$, where τ_0 represents the fluorescence lifetime of N,S CQDs (approximately in nanosecond ranges for typical CQDs). The calculated K_q values (approximately 10^{13} to 10^{14} M^{-1} s^{-1}) substantially exceeded the maximum diffusion-controlled quenching rate constant in aqueous solution (2.0×10^{10} M^{-1} s^{-1}), providing additional confirmation that the quenching process occurs through static complex formation rather than dynamic collisional encounters. These results conclusively demonstrate that vibegron interacts with N,S CQDs through static quenching involving the formation of non-fluorescent ground-state complexes.

Thermodynamic parameters governing the interaction between vibegron and N,S CQDs were determined to gain

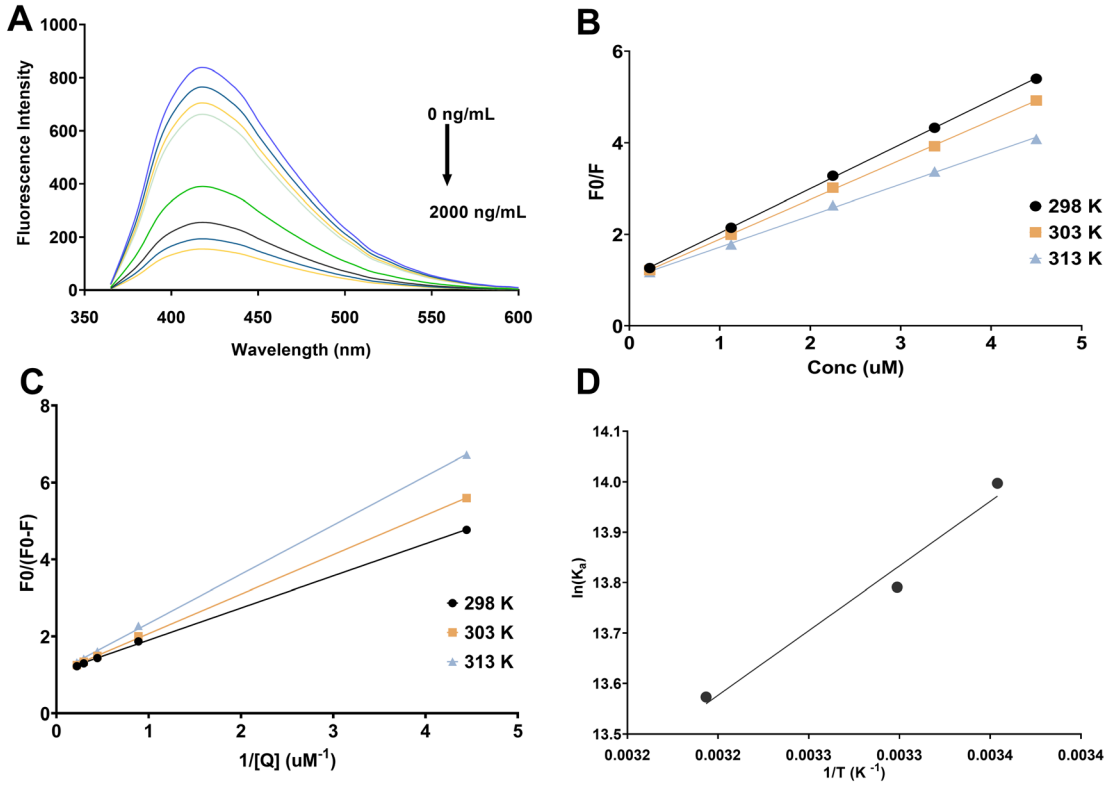

Fig. 2 (A) Fluorescence emission spectra of N,S CQDs upon addition of increasing vibegron concentrations (0–2000 ng mL^{-1}) at $\lambda_{ex} = 344$ nm, showing progressive decrease in fluorescence intensity at 418 nm; (B) Stern–Volmer plots at three different temperatures (298 K, 303 K, and 313 K) demonstrating linear relationships between F0F and vibegron concentration; (C) Modified Stern–Volmer plots for determination of association constants (K_a) at different temperatures; (D) van't Hoff plot (ln K_a *vs.* 1/T) for calculation of thermodynamic parameters ($\Delta H°$ and $\Delta S°$).

insights into the binding forces and spontaneity of complex formation. The association constant (K_a) at different temperatures was calculated using the modified Stern–Volmer equation. The modified Stern–Volmer plots exhibited good linearity at all three temperatures (Fig. 2C), and K_a values were calculated, yielding 1.20×10^6, 0.98×10^6, and 0.78×10^6 M^{-1} at 298, 303, and 313 K, respectively (Table 1). The decrease in K_a with increasing temperature further corroborates the static quenching mechanism and indicates weakening of the interaction at elevated temperatures. The thermodynamic parameters, including enthalpy change ($\Delta H°$), entropy change ($\Delta S°$), and Gibbs free energy change ($\Delta G°$), were subsequently calculated using the van't Hoff equation: $\ln K_a = -\Delta H°/R_T + \Delta S°/R$ and $\Delta G° = \Delta H° - T\Delta S°$, where R is the universal gas constant and T is the absolute temperature. The van't Hoff plot of ln K_a *versus* 1/T demonstrated excellent linearity (Fig. 2D), from which $\Delta H°$ and $\Delta S°$ were determined as −21.95 kJ mol^{-1} and 42.76 J mol^{-1} K^{-1}, respectively. The negative $\Delta G°$ values at all three temperatures (−34.70, −34.76, and −35.34 kJ mol^{-1} at 298, 303, and 313 K, respectively) indicate that the interaction between vibegron and N,S CQDs is thermodynamically spontaneous. The negative $\Delta H°$ value suggests that the binding process is exothermic, while the positive $\Delta S°$ value reflects increased randomness at the solid–liquid interface upon complex formation, likely due to the release of water molecules from the hydration shells surrounding both the N,S CQDs and vibegron during binding. According to established thermodynamic criteria, the combination of negative $\Delta H°$ and positive $\Delta S°$ typically indicates that electrostatic interactions and hydrogen bonding are the predominant driving forces for the association between vibegron and N,S CQDs. These thermodynamic insights confirm that the fluorescence quenching mechanism involves spontaneous formation of stable ground-state complexes through multiple non-covalent interactions, providing a robust basis for the analytical application of this sensing system.

Table 1 Stern–Volmer quenching constants, association constants, and thermodynamic parameters for N,S CQDs-vibegron interaction at different temperatures

Temperature (K)	K_{sv} (10^5 M^{-1})	K_a (10^6 M^{-1})	ΔG (kJ mol^{-1})	ΔH (kJ mol^{-1})	ΔS (J mol^{-1} K^{-1})
298	9.68	1.20	−34.70	−21.95	42.76
303	8.65	0.98	−34.76		
313	6.86	0.78	−35.34		

Table 2 Analysis of variance (ANOVA) results for the reduced quadratic model

Source	Sum of squares	df	Mean square	*F*-value	*p*-value	
Model	32.13	8	4.02	165.52	< 0.0001	Significant
A-pH	2.58	1	2.58	106.49	< 0.0001	
B-buffer volume	1.50	1	1.50	62.03	< 0.0001	
C–N,S CQDs	4.59	1	4.59	189.21	< 0.0001	
AC	2.21	1	2.21	91.27	< 0.0001	
BC	1.12	1	1.12	46.17	< 0.0001	
A^2	3.05	1	3.05	125.54	< 0.0001	
B^2	1.25	1	1.25	51.53	< 0.0001	
C^2	0.3221	1	0.3221	13.28	0.0019	
Residual	0.4367	18	0.0243			
Lack of fit	0.3950	16	0.0247	1.18	0.5519	Not significant
Pure error	0.0417	2	0.0208			
Cor total	32.57	26				

3.3 Optimization of experimental parameters

Prior to implementing the face-centered central composite design, preliminary scouting experiments were conducted to establish rational parameter ranges and buffer conditions for optimization. Britton–Robinson buffer (0.04 M) was selected as it provides universal pH coverage (3.0–8.0) with consistent buffering capacity across the entire range, whereas individual buffers would require multiple systems with varying ionic strengths. The pH range of 3.0–8.0 was selected as pH < 3.0 caused N,S CQD aggregation with complete fluorescence loss, while pH > 8.0 reduced quenching efficiency due to vibegron deprotonation. Buffer volume range (0.5–1.5 mL) was determined as volumes <0.5 mL caused pH drift (±0.3 units), while volumes >1.5 mL reduced baseline fluorescence. N,S CQDs concentration range (50–150 μg mL^{-1}) was established since concentrations <50 μg mL^{-1} yielded insufficient signal, while concentrations >150 μg mL^{-1} exhibited inner filter effects and self-quenching.

A face-centered central composite design was then implemented to systematically optimize the critical experimental parameters influencing the fluorescence quenching response of the N,S CQD-based sensing platform. Four independent variables were investigated within specified ranges: pH (Factor *A*: 3.0–8.0), buffer volume (Factor *B*: 0.5–1.5 mL), N,S CQDs concentration (Factor *C*: 50–150 μg mL^{-1}), and incubation time (Factor *D*: 3–15 minutes). Each factor was examined at three levels (low, center, and high), generating a total of 27 experimental runs that encompassed factorial points, axial points, and replicated center points to enable comprehensive evaluation of main effects, interaction effects, and quadratic terms (Table S1). The fluorescence quenching factor (F_0/F) served as the response variable for optimization, as it directly correlates with analytical sensitivity. This design demonstrates significant methodological advantage over traditional one-variable-at-a-time approaches commonly employed in CQD-based methods, achieving comprehensive four-factor optimization through only 27 strategically designed experiments while identifying critical interaction effects that sequential optimization cannot detect.

Statistical analysis of the experimental data identified a reduced quadratic model as the most appropriate mathematical representation of the relationship between the factors and response. Analysis of variance (ANOVA) was performed to assess the statistical significance of the developed model (Table 2). The model exhibited high statistical significance ($p < 0.05$), indicating that the selected factors substantially influence the fluorescence quenching response. Individual factor analysis revealed that pH (Factor *A*), buffer volume (Factor *B*), and N,S CQDs concentration (Factor *C*) exerted statistically significant effects on the response ($p < 0.05$), whereas incubation time (Factor *D*) demonstrated negligible influence and was consequently excluded from the final model. Furthermore, the interaction terms AC (pH × N,S CQDs concentration) and BC (buffer volume × N,S CQDs concentration) showed significant effects ($p < 0.05$), indicating synergistic relationships between these factors. The quadratic terms A^2, B^2, and C^2 were also highly significant ($p < 0.05$), confirming the non-linear nature of the response surface and justifying the use of a quadratic model.

Model validation was accomplished through rigorous diagnostic evaluation. The model demonstrated excellent fit quality, as evidenced by the high coefficient of determination (R^2 = 0.9866) and adjusted R^2 (0.9806), indicating that 98.66% of the variability in the response could be explained by the model (Table S2). The predicted R^2 value (0.9679) showed satisfactory agreement with the adjusted R^2, with a difference of less than 0.2, confirming the model's predictive capability. The adequate precision value of 33.54, substantially exceeding the desirable threshold of 4, demonstrated an adequate signal-to-noise ratio for design space navigation. Lack-of-fit analysis yielded a non-significant *p*-value (0.5519), indicating that the model adequately fits the experimental data without significant systematic error. Diagnostic plots further validated model adequacy (Fig. S3): the normal probability plot of residuals (Fig. S3A) exhibited approximate linearity, confirming normal distribution of residuals; the predicted *versus* actual values plot (Fig. S3B) demonstrated strong correlation along the 45° line; the residuals *versus* run plot (Fig. S3C) showed random scatter without apparent patterns; and the leverage *versus* run plot (Fig. S3D) indicated absence of influential outliers.

The final empirical model equation expressed in terms of coded factors was established as: F_0/F = +4.11 + 0.3789 A +

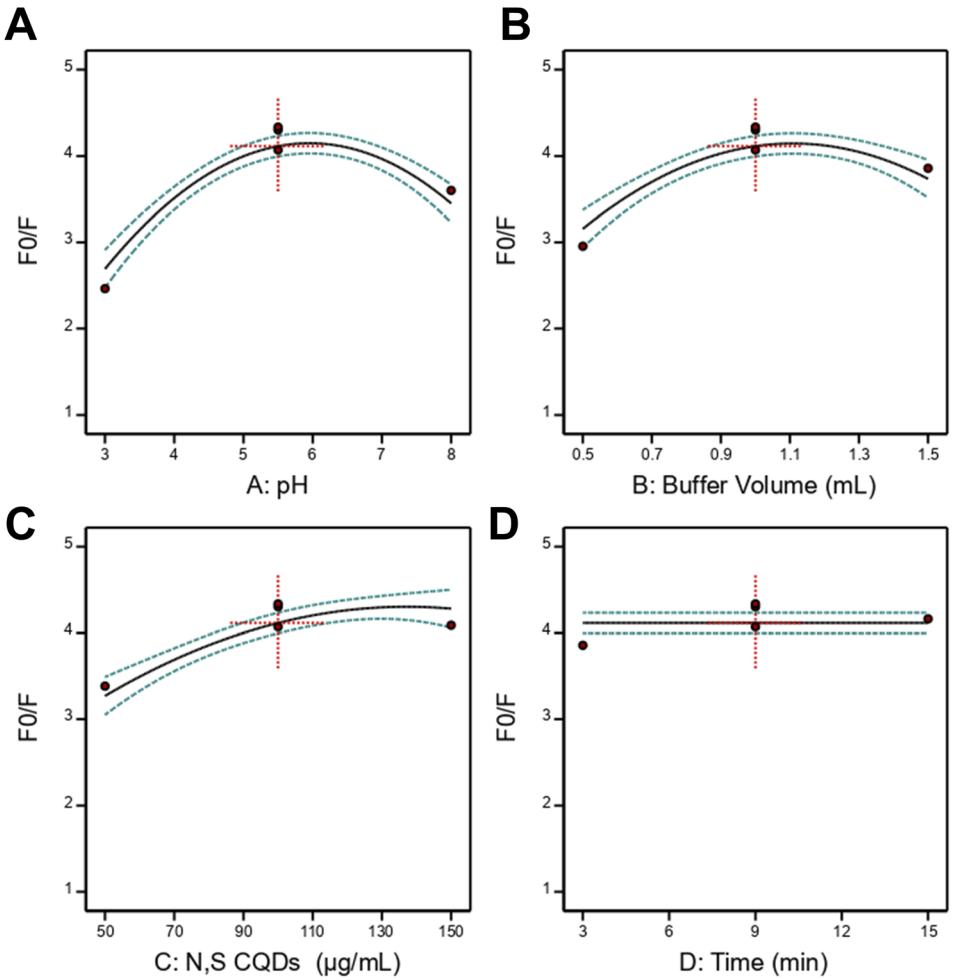

Fig. 3 Individual factor effect plots from face-centered central composite design showing the influence of experimental parameters on fluorescence quenching factor (F0/F). (A) Effect of pH (3.0–8.0); (B) Effect of buffer volume (0.5–1.5 mL); (C) Effect of N,S CQDs concentration (50–150 µg mL^{-1}); (D) Effect of incubation time (3–15 minutes).

$0.2892\,B + 0.5050\,C + 0.3720\,AC + 0.2646BC - 1.04\,A^2 - 0.6682\,B^2 - 0.3392\,C^2$. Analysis of the regression coefficients provided mechanistic insights into factor influences. The positive linear coefficients for pH (+0.3789), buffer volume (+0.2892), and N,S CQDs concentration (+0.5050) indicated that increasing these factors enhanced the fluorescence quenching factor within the experimental domain. Among the three significant factors, N,S CQDs concentration exhibited the largest coefficient magnitude, demonstrating its predominant influence on analytical sensitivity. The positive interaction coefficients (AC: +0.3720; BC: +0.2646) revealed synergistic effects, wherein the combined influence of pH with N,S CQDs concentration and buffer volume with N,S CQDs concentration exceeded their individual contributions. The negative quadratic coefficients (A^2: −1.04; B^2: −0.6682; C^2: −0.3392) indicated the presence of optimal values for each factor, beyond which further increases resulted in diminished response. Individual factor effect plots (Fig. 3A–D) corroborated these findings, displaying parabolic relationships for pH, buffer volume, and N,S CQDs concentration, with maximum responses observed at intermediate levels, while incubation time showed minimal effect across the investigated range. Importantly, the significant pH effect provides direct evidence for the electrostatic nature of the quenching mechanism. At the optimal pH of 5.6, N,S CQDs surface carboxylic acid groups (–COOH, $pK_a \approx 4.5$) are predominantly deprotonated to form anionic carboxylate groups ($–COO^-$), while amino groups ($–NH_2$) remain partially protonated. Simultaneously, vibegron containing a tertiary amine group ($pK_a \approx 9.2$) exists predominantly in its protonated cationic form. This pH-dependent ionization creates optimal conditions for electrostatic attraction between the negatively charged N,S CQDs surface and the positively charged vibegron molecule, facilitating ground–state complex formation through ion–pair interactions consistent with the thermodynamic parameters ($\Delta H^\circ = -21.95$ kJ mol^{-1}, $\Delta S^\circ = 42.76$ J mol^{-1} K^{-1}). The negative quadratic coefficient for pH (A^2: −1.04, $p < 0.0001$) confirms the existence of an optimal pH value, as deviations in either direction compromise electrostatic interactions: at pH < 4.0, excessive protonation of N,S CQDs carboxylate groups reduces negative surface charge, while at pH > 7.0, progressive deprotonation of vibegron diminishes its positive charge, both leading to decreased quenching efficiency.

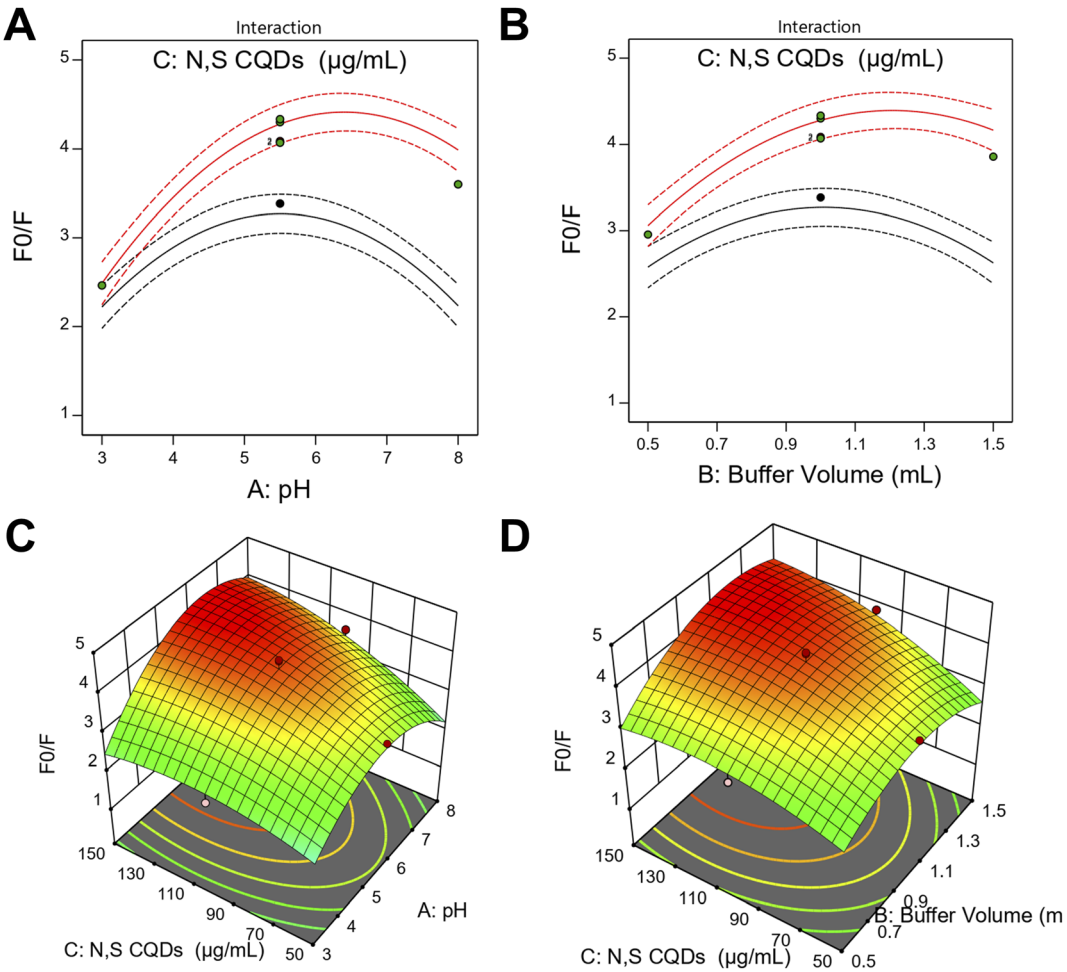

Fig. 4 Two-dimensional interaction plots and three-dimensional response surface plots from face-centered central composite design optimization. (A) Two-dimensional interaction plot showing the combined effect of pH and N,S CQDs concentration on F_0/F; black line represents N,S CQDs concentration at 50 µg mL^{-1}, red line represents 150 µg mL^{-1}, with buffer volume held constant at 1.0 mL. (B) Two-dimensional interaction plot illustrating the combined effect of buffer volume and N,S CQDs concentration on F_0/F; black line represents N,S CQDs concentration at 50 µg mL^{-1}, red line represents 150 µg mL^{-1}, with pH held constant at 5.5. (C) Three-dimensional response surface plot depicting the interaction between pH (Factor *A*) and N,S CQDs concentration (Factor *C*) with corresponding contour projection; (D) Three-dimensional response surface plot showing the interaction between buffer volume (Factor *B*) and N,S CQDs concentration (Factor *C*) with corresponding contour projection. Dotted lines represent 95% confidence intervals.

Two-dimensional interaction plots and three-dimensional response surface plots were constructed to visualize the interactive effects of significant factors on the fluorescence quenching response (Fig. 4). The two-dimensional interaction plots (Fig. 4A and B) illustrated the interaction between pH and N,S CQDs concentration, as well as buffer volume and N,S CQDs concentration, displaying curved lines characteristic of significant quadratic and interaction effects. The interaction plot for pH and N,S CQDs concentration (Fig. 4A) revealed that maximum response was achieved at intermediate levels of both factors, with the highest F_0/F values occurring at pH approximately 5.6 combined with N,S CQDs concentration near 135 µg mL^{-1}. Similarly, the interaction plot for buffer volume and N,S CQDs concentration (Fig. 4B) demonstrated optimal response at buffer volume around 1.1 mL with elevated N,S CQDs concentration. The corresponding three-dimensional response surface plots (Fig. 4C and D) provided enhanced visualization of these interactions, displaying pronounced curved surfaces with well-defined maxima. The interaction between pH and N,S CQDs concentration (Fig. 4C) exhibited a dome-shaped surface, confirming the synergistic effect where optimal fluorescence quenching was achieved through simultaneous optimization of both parameters. The buffer volume and N,S CQDs concentration interaction surface (Fig. 4D) showed similar curvature patterns, validating the importance of optimizing these factors concurrently to maximize analytical performance.

Numerical optimization was performed using the desirability function approach to identify experimental conditions that maximize the fluorescence quenching factor. The optimization ramp display (Fig. S4) illustrated the individual desirability functions for each factor, showing the optimal factor settings that achieve maximum overall desirability. The optimization algorithm generated optimal conditions of pH 5.61, buffer volume 1.04 mL, N,S CQDs concentration 133.5 µg mL^{-1},

and incubation time 3.2 minutes, yielding a predicted maximum F_0/F value with overall desirability of 1.000. For practical application, these values were rounded to pH 5.6, buffer volume 1.0 mL, N,S CQDs concentration 135 μg mL^{-1}, and incubation time 3.0 minutes. The overlay plot (Fig. S5) provided a visual representation of the design space regions satisfying the optimization criteria, with the yellow feasible region indicating where the response meets the desired specifications. Experimental validation under these rounded optimized conditions demonstrated excellent agreement with the predicted value, confirming the reliability of the developed model for method optimization. These practical optimized conditions were subsequently employed for all analytical method validation studies and real sample applications.

3.4 Method validation

The developed N,S CQDs-based spectrofluorimetric method was rigorously validated according to ICH Q2 (R2) guidelines[45] to ensure reliability, accuracy, and suitability for routine pharmaceutical analysis (Table 3).

Linearity was established by analyzing vibegron standard solutions at seven concentration levels ranging from 30 to 1500 ng mL^{-1}. The calibration curve, constructed by plotting the fluorescence quenching factor (F_0/F) against vibegron concentration, exhibited excellent linearity with a correlation coefficient (r^2) of 0.9998, demonstrating a strong linear relationship between the response and analyte concentration. The regression equation was determined as $F_0/F = 0.0022$ [Vibegron] + 1.0583, where [Vibegron] represents the concentration in ng mL^{-1}. Method sensitivity was assessed through determination of the limit of detection (LOD) and limit of quantification (LOQ) according to ICH guidelines. The calculated LOD was 9.85 ng mL^{-1}, while the LOQ was established at 29.54 ng mL^{-1}, indicating high sensitivity suitable for trace-level quantification of vibegron in pharmaceutical formulations and biological matrices (Table 3). These sensitivity parameters are superior to previously reported HPLC-PDA methods and comparable to the spectrofluorimetric derivatization method, while offering advantages of simplicity and rapidity.

Table 3 Analytical performance parameters of the developed spectrofluorimetric method for vibegron determination

Parameters		Vibegron
Excitation wavelength (nm)		344
Emission wavelength (nm)		418
Linearity range (ng mL^{-1})		30–1500
Slope		0.0022
Intercept		1.0583
Correlation coefficient (r^2)		0.9998
LOD (ng mL^{-1})		9.85
LOQ (ng mL^{-1})		29.54
Accuracy (% R)[a]		100.88 ± 1.339
Repeatability precision (% RSD)[b]		1.328
Intermediate precision (% RSD)[c]		1.737
Robustness (% R)	Buffer (pH)	100.05 ± 0.914
	Reagent conc. (μg mL^{-1})	98.55 ± 1.254
	Reaction time (min)	99.83 ± 0.982

[a] Average of 9 determinations (3 concentrations repeated 3 times). [b] % RSD of 9 determinations (3 concentrations repeated 3 times) measured on the same day. [c] % RSD of 9 determinations (3 concentrations repeated 3 times) measured in the three consecutive days.

Method accuracy was evaluated through recovery studies by analyzing vibegron standard solutions at three concentration levels within the linearity range, with each level analyzed in triplicate. The mean recovery was 100.88 ± 1.34%, demonstrating excellent accuracy with minimal systematic error (Table 3). Precision was assessed at two levels: repeatability (intra-day precision) and intermediate precision (inter-day precision). Repeatability was evaluated by analyzing three different concentrations in triplicate on the same day, yielding a relative standard deviation (RSD) of 1.33%, indicating excellent measurement reproducibility. Intermediate precision was assessed by repeating the same measurements on three consecutive days, resulting in an RSD of 1.74%. Method robustness was evaluated by deliberately introducing minor variations to critical experimental parameters, including pH (5.6 ± 0.2), N,S CQDs concentration (135 ± 5 μg mL^{-1}), and incubation time (3.0 ± 0.5 minutes). The recovery percentages remained within acceptable limits for all tested variations: buffer pH (100.05 ± 0.91%), reagent concentration (98.55 ± 1.25%), and reaction time (99.83 ± 0.98%), demonstrating that the method remains reliable despite small deviations in experimental conditions during routine analysis.

Selectivity was comprehensively validated through systematic evaluation of 13 potential interferents representing pharmaceutical excipients and endogenous biological components (Table S3). Pharmaceutical excipients were tested at 10-fold molar excess relative to vibegron (1500 ng mL^{-1}) to ensure detection of any potential interference under high excipient load conditions. Biological components were examined at upper physiological concentration limits: glucose (100 mg dL^{-1}), urea (50 mg dL^{-1}), uric acid (8 mg dL^{-1}), creatinine (2 mg dL^{-1}), albumin (5 g dL^{-1}), ascorbic acid (2 mg dL^{-1}), and cholesterol (300 mg dL^{-1}). Critical control experiments were performed to assess direct fluorescence effects of interferents in the absence of vibegron. Each interferent was added to N,S CQD solutions without vibegron to measure baseline fluorescence intensity (F_0). All tested substances showed negligible effects on baseline fluorescence, with changes ranging from −0.8% to +0.5% relative to blank N,S CQD solutions, confirming absence of intrinsic fluorescence or quenching properties. Subsequently, interference effects were evaluated in the presence of vibegron (1500 ng mL^{-1}). All pharmaceutical excipients at 10-fold molar excess demonstrated quenching efficiencies ranging from 76.45% to 77.31%, statistically equivalent to vibegron alone (76.90%, RSD = 1.54%). The maximum deviation was +0.38% for magnesium stearate and −0.45% for ascorbic acid, both well within acceptable analytical variation (<3%). Biological components exhibited similarly negligible interference, with quenching efficiencies of 76.58–77.31%. These results collectively confirm high method selectivity, demonstrating that fluorescence quenching response is specific to vibegron and unaffected by common pharmaceutical excipients or endogenous plasma components at physiologically relevant

Table 4 Statistical comparison of the developed method with the reported HPLC method for vibegron determination in pharmaceutical tablets

Method	Mean[a]	SD	t-test (2.306)[b]	P value	F-value (6.338)[b]	P value	θ_L [c]	θ_U [c]
Developed method	100.07	0.814	0.175	0.866	1.908	0.547	−1.540	1.322
Reported method	100.18	1.124						

[a] Average of five determinations. [b] The values in parenthesis are tabulated values of "t "and "F" at ($P = 0.05$). [c] Bias of ± 2% is acceptable.

concentrations. However, it should be acknowledged that structurally similar compounds containing aromatic rings, amino groups, or electron-rich moieties may potentially interact with N,S CQDs through similar mechanisms, representing a common limitation of spectrofluorimetric sensors based on non-specific molecular interactions. This challenge is inherent to fluorescence-based sensing platforms and can be addressed through several approaches, including incorporation of molecularly imprinted polymers (MIPs) to enhance selectivity, or implementation of appropriate sample preparation techniques such as solid-phase extraction or liquid-liquid extraction to separate the analyte of interest from potential interferents prior to analysis. For the intended application to vibegron quantification in pharmaceutical formulations and biological samples, where structurally similar β3-adrenergic agonists are unlikely to be co-administered, the demonstrated selectivity profile is considered adequate for practical analytical purposes.

3.5 Application to real samples

The validated N,S CQDs-based spectrofluorimetric method was successfully applied to the quantification of vibegron in commercial pharmaceutical formulations and spiked human plasma samples to assess its practical applicability. Ten tablets were analyzed following the sample preparation procedure described previously and the mean vibegron content was determined to be 100.07 ± 0.81% of the labeled claim ($n = 5$), demonstrating excellent agreement with the nominal value and confirming the accuracy of the developed method for pharmaceutical quality control applications (Table 4). The low relative standard deviation (0.81%) indicated high precision in tablet analysis, reflecting the robustness of the method in complex pharmaceutical matrices despite the presence of various excipients.

To establish the reliability and equivalence of the developed method with established analytical techniques, statistical comparison was performed against a reported HPLC method[12] for vibegron determination (Table 4). Student's t-test was applied to compare the means obtained by both methods, yielding a calculated t-value of 0.175, which was substantially lower than the tabulated critical value of 2.306 at the 95% confidence level ($p = 0.866$). This result indicated no significant difference between the two methods in terms of accuracy. The F-test was employed to compare the precision of both methods, with a calculated F-value of 1.908, well below the critical value of 6.338, demonstrating comparable precision between the developed and reference methods ($p = 0.547$). Furthermore, interval hypothesis testing was conducted to assess method equivalence, with acceptance limits set at ±2% bias. The calculated confidence interval ($\theta_L = -1.540$, $\theta_U = 1.322$) fell entirely within the acceptance range, confirming that the developed method is equivalent to the established HPLC method (Table 4). These statistical evaluations collectively demonstrated that the proposed N,S-CQD-based fluorescence quenching method provides results comparable to conventional chromatographic techniques while offering advantages of simplified sample preparation, reduced analysis time, and lower operational costs.

The applicability of the developed method to biological matrices was evaluated through analysis of drug-free human plasma samples spiked with known concentrations of vibegron at four levels: 50, 100, 300, and 600 ng mL^{-1} (Table 5). Prior to recovery studies, the acetonitrile volume for protein precipitation was optimized by investigating acetonitrile-to-plasma ratios of 1 : 1, 2 : 1, 3 : 1, and 4 : 1 (v/v) using spiked samples at 300 ng mL^{-1}. The optimal ratio of 2 : 1 (2 mL acetonitrile per 1 mL plasma) was selected as it provided complete protein precipitation with clear supernatants and maximum analyte recovery (102.03 ± 2.39%), while lower ratios resulted in incomplete precipitation (turbid supernatants, recoveries 82–88%) and higher ratios offered no additional benefit while increasing solvent consumption. From a green chemistry perspective, the 2 : 1 ratio represents the minimum acetonitrile volume required for effective deproteinization, thereby aligning with principles of solvent minimization. Following the optimized protein precipitation and sample preparation protocol, recovery studies were conducted in triplicate for each concentration level. The mean recovery percentages were 104.28%, 96.44%, 103.03%, and 101.17% for the 50, 100, 300, and 600 ng mL^{-1} spiking levels, respectively, with corresponding RSD values of 4.00%, 2.93%, 2.38%, and 1.99%. These results demonstrated satisfactory accuracy and precision across the tested concentration range, with all recovery values falling within the range of 96–105% and RSD values below 5%, meeting the criteria for bioanalytical method validation. The slightly higher RSD at the lowest concentration (50 ng mL^{-1}) can be attributed to the proximity to the LOQ and the inherent

Table 5 Recovery studies for vibegron determination in spiked human plasma samples at four concentration levels ($n = 3$)

Spiked (ng mL^{-1})	Found (ng mL^{-1})	Recovery (%)	RSD ($n = 3$%)
50	52.14	104.28	3.999
100	96.44	96.44	2.925
300	309.09	103.03	2.379
600	607.03	101.17	1.992

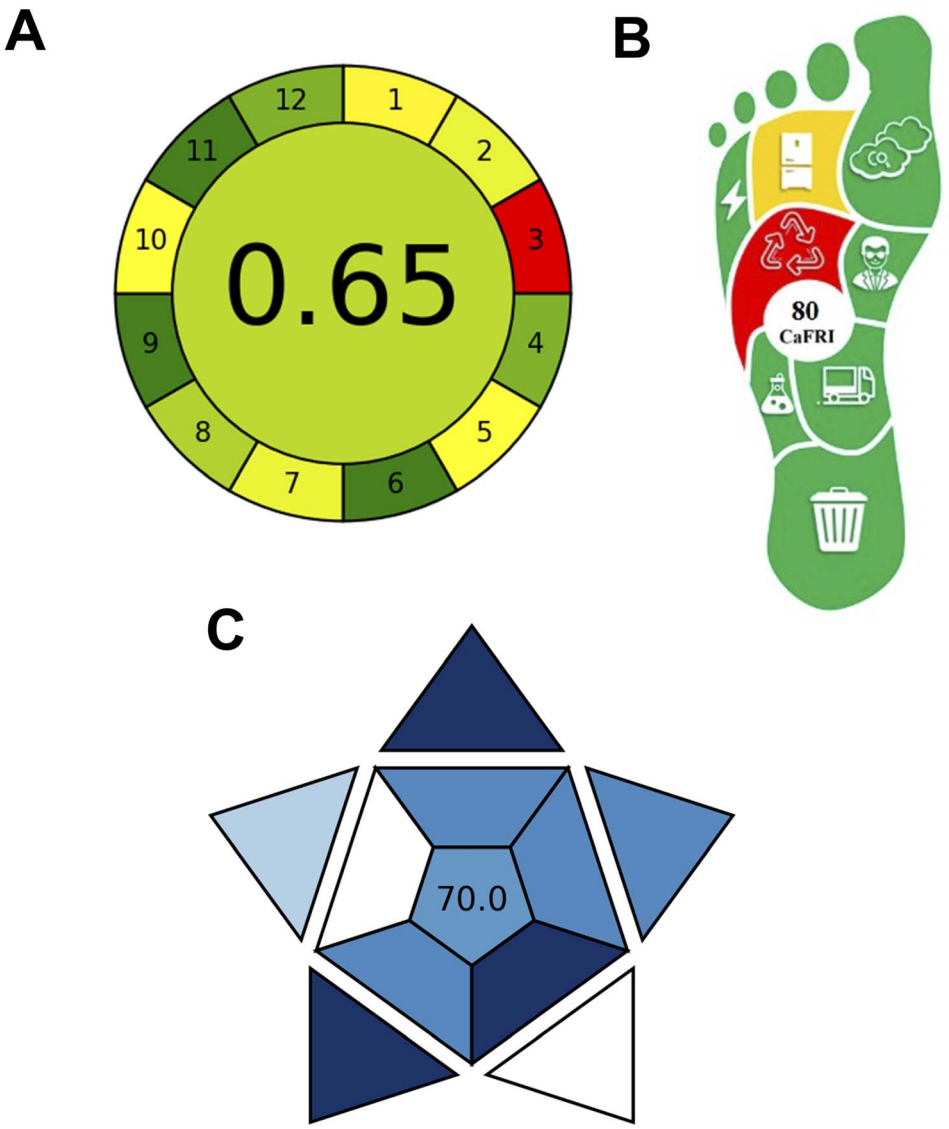

Fig. 5 Green chemistry assessment of the developed method. (A) AGREE (Analytical GREEnness metric) pictogram showing overall score of 0.65 with twelve segments representing the twelve principles of green analytical chemistry; (B) CaFRI (Carbon Footprint Reduction Index) pictogram in the shape of a foot displaying a score of 80/100; (C) BAGI (Blue Applicability Grade Index) asteroid-shaped pictogram showing a score of 70.0/100, with ten sections representing practical applicability attributes.

variability associated with sample preparation procedures for biological matrices. The successful application to plasma samples confirms the suitability of the developed method for therapeutic drug monitoring and pharmacokinetic studies of vibegron in biological fluids.

3.6 Green chemistry assessment

The environmental sustainability and greenness profile of the developed N,S CQDs-based spectrofluorimetric method were comprehensively evaluated using three complementary assessment tools: the Analytical GREEnness metric (AGREE),[40] Carbon Footprint Reduction Index (CaFRI),[41] and Blue Applicability Grade Index (BAGI).[42] AGREE was selected as the most widely accepted tool based on the twelve principles of Green Analytical Chemistry, providing comprehensive pictogram visualization of reagent usage, waste generation, and energy consumption, with extensive recent application to pharmaceutical fluorescence methods.[40,46,47] CaFRI was incorporated to specifically quantify carbon footprint and greenhouse gas emissions—a critical sustainability parameter not explicitly addressed by AGREE—evaluating electrical energy consumption, CO_2 emissions, and waste management.[41] BAGI was included to assess practical applicability complementary to environmental greenness, evaluating ten criteria including instrumentation accessibility, sample preparation complexity, and cost-effectiveness, ensuring the method is practically viable for routine implementation.[42] This multi-metric approach provides holistic evaluation encompassing environmental impact, carbon footprint, and practical applicability, aligning with recent recommendations for comprehensive sustainability assessment in pharmaceutical analysis.[48,49]

The AGREE metric, which assesses methods based on the twelve principles of green analytical chemistry, yielded an overall score of 0.65 (Fig. 5A). This score, represented by a yellow-green background in the clock-like pictogram, indicates satisfactory greenness with notable strengths in several criteria. The method achieved excellent scores (dark green segments) for principles related to avoidance of derivatization (Principle 6), energy minimization (Principle 9), and elimination of toxic reagents (Principle 11), reflecting the inherent advantages of the direct fluorescence-based detection approach without requiring hazardous chemical modifications. Good performance was also observed for integration of analytical steps (Principle 4) and operator safety (Principle 12). However, limitations were identified in the *in situ* measurement capability (Principle 3, red segment), as the method requires laboratory-based instrumentation, and modest scores were obtained for sample treatment (Principle 1), sample size (Principle 2), waste generation (Principle 7), and automation (Principle 5), indicating areas for potential future improvement through method miniaturization and automation strategies.

The CaFRI assessment, which specifically focuses on carbon footprint and greenhouse gas emissions, resulted in a score of 80 out of 100 (Fig. 5B). The foot-shaped pictogram predominantly displayed green coloration across most criteria, indicating low environmental impact. The method excelled in several categories including low electrical power consumption (0.1–1.5 kW), absence of energy-intensive equipment, favorable CO_2 emission factor, minimal waste generation (<10 mL per sample), high sample throughput (10–30 samples per hour), and limited use of hazardous reagents (≤3 pictograms, <5 mL organic solvents per sample). The primary limitation identified was the lack of reagent recycling, which represents an opportunity for further sustainability enhancement in future method iterations. The high CaFRI score confirms that the developed method significantly reduces carbon footprint compared to conventional chromatographic techniques that typically require larger volumes of organic solvents, longer analysis times, and more energy-intensive instrumentation.

The BAGI evaluation, assessing practical applicability complementary to greenness metrics, yielded a score of 70.0 out of 100 (Fig. 5C). This score was calculated by systematically evaluating ten main attributes related to method practicality, including analysis type, instrumentation requirements, sample throughput, automation degree, and reagent accessibility.[42] Each attribute contributes to the overall score based on predefined criteria, with the cumulative assessment reflecting the method's practical performance across all evaluated dimensions. The asteroid-shaped pictogram exhibited predominantly blue coloration, indicating good to excellent practical performance across multiple attributes. The method demonstrated strengths in several categories: quantitative analysis capability, simple and commercially available instrumentation (spectrofluorometer), simultaneous preparation of multiple samples (>95 samples), high throughput (>10 samples per hour), simple low-cost sample preparation without preconcentration requirements, and moderate sample volume requirements (100–500 μL). However, the manual operation mode, single-analyte focus, and requirement for in-lab synthesis of N,S CQDs (though *via* simple microwave protocol) represented areas scoring lower on the practical scale. The BAGI score above the recommended threshold of 60 confirms that the method possesses adequate practical utility for routine implementation in quality control and bioanalytical laboratories.

Collectively, these three-assessment metrics demonstrate that the developed N,SCQDs-based spectrofluorimetric method exhibits favorable environmental sustainability, low carbon footprint, and good practical applicability. The method aligns well with the principles of green analytical chemistry by minimizing hazardous reagent consumption, reducing waste generation, operating with low energy requirements, and providing rapid analysis without derivatization steps. Compared to conventional HPLC methods that typically score lower on environmental metrics due to substantial organic solvent consumption (acetonitrile-based mobile phases) and higher energy demands from extended chromatographic runs,[12,13] the proposed fluorescence-based approach offers a more sustainable alternative for vibegron quantification while maintaining comparable analytical performance. The aqueous-based chemistry, elimination of toxic organic solvents, rapid 3 minutes analysis time, and simple instrumentation collectively contribute to superior green chemistry scores (AGREE: 0.65, CaFRI: 80/100) compared to typical chromatographic methods. These findings support the adoption of this method as an environmentally friendly analytical tool suitable for routine pharmaceutical quality control and therapeutic drug monitoring applications, addressing the growing emphasis on sustainable analytical practices in pharmaceutical laboratories.

4. Conclusion

This study successfully developed and validated a novel, sensitive, and environmentally sustainable spectrofluorimetric method for vibegron quantification based on N,S CQDs as fluorescent nanoprobes. The N,S CQDs were synthesized *via* a rapid microwave-assisted green chemistry approach, exhibiting a high quantum yield of 51.36%, quasi-spherical morphology with mean particle size of 3.23 ± 1.41 nm, and excellent colloidal stability. Mechanistic investigations revealed that vibegron induced fluorescence quenching through static complex formation, as confirmed by temperature-dependent Stern–Volmer analysis and thermodynamic parameter evaluation. The interaction was driven by electrostatic forces and hydrogen bonding, characterized by negative enthalpy change ($\Delta H^\circ = -21.95$ kJ mol^{-1}) and positive entropy change ($\Delta S^\circ =$ 42.76 J mol^{-1} K^{-1}). Subsequently, systematic optimization using face-centered central composite design established optimal experimental conditions (pH 5.6, buffer volume 1.0 mL, N,S CQDs concentration 135 μg mL^{-1}, incubation time 3.0 minutes), yielding maximum analytical sensitivity with excellent model fit ($R^2 = 0.9866$).

The validated method demonstrated superior analytical performance according to ICH Q2 (R2) guidelines, with wide linearity range (30–1500 ng mL^{-1}, $r^2 = 0.9998$), high sensitivity (LOD 9.85 ng mL^{-1}, LOQ 29.54 ng mL^{-1}), excellent accuracy

(100.88 ± 1.34%), and precision (RSD < 2%). Furthermore, successful application to commercial vibegron tablets and spiked human plasma samples confirmed practical applicability, with recovery values ranging from 96.44% to 104.28%. Statistical comparison demonstrated equivalence to established HPLC methods through student's *t*-test, *F*-test, and interval hypothesis testing. Moreover, comprehensive green chemistry assessment using AGREE (0.65), CaFRI (80/100), and BAGI (70.0/100) metrics confirmed favorable environmental sustainability, characterized by minimal hazardous reagent consumption, low carbon footprint, and reduced waste generation. Consequently, the developed N,S CQDs-based spectrofluorimetric method offers significant advantages over conventional chromatographic techniques, including simplified sample preparation, reduced analysis time, lower operational costs, and superior environmental sustainability. Ultimately, this work provides a practical, cost-effective, and environmentally benign analytical tool suitable for routine quality control laboratories and therapeutic drug monitoring programs, thereby contributing to the advancement of green analytical methodologies in pharmaceutical analysis.

Conflicts of interest

There are no conflicts to declare.

Data availability

The authors confirm that the data supporting the findings of this study are available within the article and its supplementary information (SI) file. Any additional data are available from the corresponding author upon reasonable request. Supplementary information is available. See DOI: https://doi.org/10.1039/d5ra08942e.

Acknowledgements

This study is supported *via* funding from Prince sattam bin Abdulaziz University project number (PSAU/2026/R/1447).

References

1 B. T. Haylen, D. De Ridder, R. M. Freeman, S. E. Swift, B. Berghmans, J. Lee, A. Monga, E. Petri, D. E. Rizk and P. K. Sand, *Neurourol. Urodyn.*, 2010, **29**, 4–20.
2 D. E. Irwin, Z. S. Kopp, B. Agatep, I. Milsom and P. Abrams, *BJU Int.*, 2011, **108**, 1132–1138.
3 B. Peyronnet, B. M. Brucker, C. De Nunzio, C. Gratzke, J. Heesakkers, M. C. Michel, M. Serati, D. Staskin and C. Chapple, *World J. Urol.*, 2025, **43**, 1–14.
4 I. Milsom, S. A. Kaplan, K. S. Coyne, C. C. Sexton and Z. S. Kopp, *Urology*, 2012, **80**, 90–96.
5 Y. Lou, M. Cheng, Q. Cao, K. Li, H. Qin, M. Bao, Y. Zhang, S. Lin and Y. Zhang, *J. Pharm. Biomed. Anal.*, 2024, **240**, 115937.
6 S. Yamamoto, H. Kusabuka, A. Matsuzawa, I. Maruyama and T. Yamazaki, *PLoS One*, 2023, **18**, e0290685.
7 Y. Igawa, N. Aizawa and M. C. Michel, *Br. J. Pharmacol.*, 2019, **176**, 2525–2538.
8 C. R. Chapple, *Eur. Neurol.*, 2019, **75**, 283–284.
9 S. J. Keam, *Drugs*, 2018, **78**, 1835–1839.
10 J. King, A. Walker, D. Aikin, C. Haag-Molkenteller and M. Kankam, *Clin. Pharmacol. Drug Dev.*, 2022, **11**, 1349–1355.
11 S. D. Edmondson, C. Zhu, N. F. Kar, J. Di Salvo, H. Nagabukuro, B. Sacre-Salem, K. Dingley, R. Berger, S. D. Goble and G. Morriello, *J. Med. Chem.*, 2016, **59**, 609–623.
12 N. Vadnere and M. Patel, *Chromatographia*, 2025, 1–18.
13 N. Vadnere and M. Patel, *Accred Qual. Assur.*, 2025, 1–11.
14 M. Wadie, M. A. Tantawy and Z. M. Goda, *J. Fluoresc.*, 2024, 1–11.
15 S. M. Abo Elkheir, J. J. M. Nasr, M. I. Walash and A. M. Zeid, *Sci. Rep.*, 2025, **15**, 32598.
16 S. F. El-Malla, E. A. Elshenawy, S. F. Hammad and F. R. Mansour, *Anal. Chim. Acta*, 2022, **1197**, 339491.
17 Y.-P. Sun, B. Zhou, Y. Lin, W. Wang, K. S. Fernando, P. Pathak, M. J. Meziani, B. A. Harruff, X. Wang and H. Wang, *J. Am. Chem. Soc.*, 2006, **128**, 7756–7757.
18 S. Carneiro, J. Oliveira, V. Rodrigues, J. Lima, J. Do Nascimento, R. Santos-Oliveira, L. Fechine, R. Freire and P. Fechine, *Mater. Today Nano*, 2023, **22**, 100345.
19 N. Azam, M. Najabat Ali and T. Javaid Khan, *Front. Mater.*, 2021, **8**, 700403.
20 Q. Xu, T. Kuang, Y. Liu, L. Cai, X. Peng, T. S. Sreeprasad, P. Zhao, Z. Yu and N. Li, *J. Mater. Chem. B*, 2016, **4**, 7204–7219.
21 L. Ansari, S. Hallaj, T. Hallaj and M. Amjadi, *Colloids Surf., B*, 2021, **203**, 111743.
22 G. Somaraj, S. Mathew, T. Abraham, K. Ambady, C. Mohan and B. Mathew, *ChemistrySelect*, 2022, **7**, e202200473.
23 H. Qi, M. Teng, M. Liu, S. Liu, J. Li, H. Yu, C. Teng, Z. Huang, H. Liu and Q. Shao, *J. Colloid Interface Sci.*, 2019, **539**, 332–341.
24 M. Chaghaghazardi, S. Kashanian, M. Nazari, K. Omidfar, Y. Joseph and P. Rahimi, *Spectrochim. Acta Mol. Biomol. Spectrosc.*, 2023, **293**, 122448.
25 C. Wang, J. Xu, H. Li and W. Zhao, *Luminescence*, 2020, **35**, 1373–1383.
26 M. A. A. Hamid, S. H. Elagamy, A. Gamal and F. R. Mansour, *Spectrochim. Acta Mol. Biomol. Spectrosc.*, 2023, **293**, 122440.
27 Z. Yu, C. Deng, W. Ma, Y. Liu, C. Liu, T. Zhang and H. Xiao, *Nanomaterials*, 2024, **14**, 1827.
28 N. A. Qandeel, A. A. El-Masry, M. Eid, M. A. Moustafa and R. El-Shaheny, *Anal. Chim. Acta*, 2023, **1237**, 340592.
29 B. K. John, N. John and B. Mathew, 2022.
30 A. Abdel-Hakim, F. Belal, M. A. Hammad and M. El-Maghrabey, *Methods Appl. Fluoresc*, 2023, **11**, 045007.
31 Q. Fu, N. Li, K. Lu, Z. Dong and Y. Yang, *Mater. Today Chem.*, 2024, **37**, 102032.
32 G. Magdy, A. F. A. Hakiem, F. Belal and A. M. Abdel-Megied, *Food Chem.*, 2021, **343**, 128539.
33 Y. Fan, L. Shen, Y. Liu, Y. Hu, W. Long, H. Fu and Y. She, *Food Chem.*, 2023, **421**, 136105.
34 K. Sahin Tiras and N. Ertas Onmaz, *Microchem. J.*, 2025, **218**, 115232.

35 R. A. Emam, G. Magdy, F. Belal and A. A. Emam, *Microchem. J.*, 2025, **212**, 113248.
36 N. A. Qandeel, A. A. El-Masry, M. Eid, M. A. Moustafa and R. El-Shaheny, *Anal. Chim. Acta*, 2023, **1237**, 340592.
37 A. S. Radwan, G. Magdy, A. K. El-Deen, F. Belal and H. Elmansi, *Luminescence*, 2025, **40**, e70204.
38 M. Rani and U. Shanker, *Anal. Chim. Acta*, 2025, **1351**, 343904.
39 J. Zhan, R. Peng, S. Wei, J. Chen, X. Peng and B. Xiao, *ACS Omega*, 2019, **4**, 22574–22580.
40 F. Pena-Pereira, W. Wojnowski and M. Tobiszewski, *Anal. Chem.*, 2020, **92**, 10076–10082.
41 F. R. Mansour and P. M. Nowak, *BMC Chem.*, 2025, **19**, 121.
42 N. Manousi, W. Wojnowski, J. Płotka-Wasylka and V. Samanidou, *Green Chem.*, 2023, **25**, 7598–7604.
43 K. G. Nguyen, I.-A. Baragau, R. Gromicova, A. Nicolaev, S. A. Thomson, A. Rennie, N. P. Power, M. T. Sajjad and S. Kellici, *Sci. Rep.*, 2022, **12**, 13806.
44 L. Fu, Y. Yin, G. Cao, P. Wu, J. Wang, L. Yan, B. Zhang and M. Li, *Chin. Phys. B*, 2019, **28**, 128102.
45 I.C.H. Guideline, ICH: Geneva, Switzerland, 2022, 1.
46 M. Ahmed, E. Eiman, K. M. Al-Ahmary, F. Aftab, A. Sohail, H. Raza and I. Ali, *Microchem. J.*, 2024, **205**, 111400.
47 L. Yin, L. Yu, Y. Guo, C. Wang, Y. Ge, X. Zheng, N. Zhang, J. You, Y. Zhang and M. Shi, *J. Pharm. Anal.*, 2024, **14**, 101013.
48 M. Mehta, D. Mehta and R. Mashru, *Future J. Pharmaceut. Sci.*, 2024, **10**, 83.
49 S. M. Miladinović, *Anal. Bioanal. Chem.*, 2025, **417**, 665–673.